Biophysical Journal Volume 109 December 2015 2666–2677

Article

Mechanism of Protein Denaturation: Partial Unfolding of the P22 Coat Protein I-Domain by Urea Binding

Rebecca L. Newcomer,[1] LaTasha C. R. Fraser,[1] Carolyn M. Teschke,[1,2,*] and Andrei T. Alexandrescu[1,*]

[1]Department of Molecular and Cell Biology and [2]Department of Chemistry, University of Connecticut, Storrs, Connecticut

ABSTRACT The I-domain is an insertion domain of the bacteriophage P22 coat protein that drives rapid folding and accounts for over half of the stability of the full-length protein. We sought to determine the role of hydrogen bonds (H-bonds) in the unfolding of the I-domain by examining $^{3}J_{NC'}$ couplings transmitted through H-bonds, the temperature and urea-concentration dependence of ^{1}HN and ^{15}N chemical shifts, and native-state hydrogen exchange at urea concentrations where the domain is predominantly folded. The native-state hydrogen-exchange data suggest that the six-stranded β-barrel core of the I-domain is more stable against unfolding than a smaller subdomain comprised of a short α-helix and three-stranded β-sheet. H-bonds, separately determined from solvent protection and $^{3}J_{NC'}$ H-bond couplings, are identified with an accuracy of 90% by ^{1}HN temperature coefficients. The accuracy is improved to 95% when ^{15}N temperature coefficients are also included. In contrast, the urea dependence of ^{1}HN and ^{15}N chemical shifts is unrelated to H-bonding. The protein segments with the largest chemical-shift changes in the presence of urea show curved or sigmoidal titration curves suggestive of direct urea binding. Nuclear Overhauser effects to urea for these segments are also consistent with specific urea-binding sites in the I-domain. Taken together, the results support a mechanism of urea unfolding in which denaturant binds to distinct sites in the I-domain. Disordered segments bind urea more readily than regions in stable secondary structure. The locations of the putative urea-binding sites correlate with the lower stability of the structure against solvent exchange, suggesting that partial unfolding of the structure is related to urea accessibility.

INTRODUCTION

Capsid shells that protect viral genomes are assembled from multiple copies of coat proteins with highly conserved folds (1–3). The HK97-fold, named after the first known structural example from Hong Kong 97 virus (4), is shared by the coat proteins of tailed double-stranded DNA viruses and phages that form capsids with diameters ranging from 45 to 187 nm (1,5). The HK97-fold is found in the coat proteins of more than 40 phages and viruses, including P22, λ, T7, and Herpes simplex virus 1 (1). Presumably to increase their functional versatility, some of the coat proteins based on the HK97 motif contain additional inserted domains (I-domains) (1,6–10).

The I-domain from phage P22's coat protein, the subject of this study, has a bipartite structure consisting of a six-stranded, Greek key, β-barrel core flanked by a smaller accessory subdomain comprised of three short β-strands and an α-helix (8). The β-barrel of the I-domain shows structural homology to the β-barrel from a translation factor domain (8). Like the I-domain, the translation factor domain has a smaller subdomain consisting of a short α-helix and three β-strands. In contrast to the structurally homologous β-barrels that superpose with a backbone root mean-square deviation of 2.6 Å, the smaller accessory domains are not structurally conserved (8). Two long loops, called the S- and D-loops (6,8), are disordered in the isolated I-domain and in the full-length coat protein, but become structured to form salt bridges between capsomers when the coat protein assembles into capsids (8). In addition to its role in capsid assembly, the multifunctional I-domain acts as a folding nucleus and stabilizes the full-length coat protein (11). The I-domain is the site for many of the P22 coat protein mutations that confer a temperature-sensitive folding (*tsf*) phenotype, allowing coat protein folding and assembly at permissive temperatures but causing coat protein aggregation at higher temperatures (8,12). We proposed that the I-domain is an uncleaved intramolecular chaperone that functions via thermodynamic, rather than kinetic, control of folding (13).

In an effort to better understand the folding properties of the I-domain, we characterized hydrogen exchange (HX) as a function of urea concentration under conditions in which the native state is populated in excess of 99%. In this approach, called native-state HX (NSHX) (14), amide protons exchange with solvent protons through transiently formed partially or globally unfolded conformations that become increasingly populated with increasing concentrations of denaturant (14). The NSHX experiment thus

Submitted August 19, 2015, and accepted for publication November 6, 2015.

*Correspondence: andrei.alexandrescu@uconn.edu or carolyn.teschke@uconn.edu

Rebecca L. Newcomer and LaTasha C. R. Fraser contributed equally to this work.

Editor: H. Jane Dyson.

0006-3495/15/12/2666/12

http://dx.doi.org/10.1016/j.bpj.2015.11.010

provides information about the global stability of a protein and can identify partially unfolded states (14–17). In addition to the NSHX experiments, we investigated hydrogen bonding (H-bonding) in the I-domain using 3D long-range HNCO (lrHNCO) NMR spectroscopy (18), which identifies H-bond donors and acceptors through small $J_{NC'}$ couplings transmitted through H-bonds (18–21). We also measured the temperature dependence of ^{1}HN and ^{15}N chemical shifts to obtain temperature coefficients that are predictive of H-bonding (22–24).

Our analysis of the urea dependence of ^{1}H and ^{15}N chemical shifts together with 3D nuclear Overhauser effect spectroscopy/heteronuclear single-quantum correlation (NOESY-HSQC) spectroscopy suggests that the least stable regions of the I-domain determined by the NSHX experiment correspond to sites in the protein that most readily bind urea. Rather than perturbing the solvent structure, urea appears to actively drive unfolding by penetrating the I-domain and disrupting H-bonds. Together, these studies shed light on the stability hierarchy of H-bonded structures in the I-domain, interactions between the I-domain and urea, and how denaturants such as urea may unfold proteins.

MATERIALS AND METHODS

Materials

I-domain isotopically enriched with ^{15}N was expressed in *Escherichia coli* BL21(DE3) cells containing the *pET30b* plasmid with an inserted gene fragment encoding residues S223–V345 of full-length P22 coat protein (8,25). Samples for NMR experiments were purified as previously described (8,25). D_2O for HX studies (99.96%) was obtained from Cambridge Isotope Laboratories (Tewksbury, MA). Urea (molecular biology grade, >99% pure) was obtained from Fisher Scientific (Pittsburgh, PA). The concentrations of all urea solutions were determined by refractometry (26).

Urea denaturation by circular dichroism

Circular dichroism (CD) experiments were performed using a Pi-Star 180 spectropolarimeter from Applied Photophysics (Leatherhead, UK). I-domain solutions were diluted to a final protein concentration of 0.2 mg/mL in 20 mM sodium phosphate buffer (pH 6.0) and mixed using a Microlab 50 Titrator (Hamilton, Franklin, MA) to final urea concentrations ranging from 0 to 6 M. Samples were incubated for 3 h at 25°C, and the CD signal was averaged for 20 scans at 220 nm using a 4-nm slit width and a 2.0-mm-pathlength cell. ΔG_{spec}-values were calculated using a six-parameter nonlinear least-squares fit of the CD titration data as previously described (27).

NMR spectroscopy

NMR data were collected on a 600 MHz Varian Inova spectrometer equipped with a cryogenic probe. Unless otherwise noted, all NMR experiments were performed at 25°C with ^{15}N-labeled samples of the I-domain in aqueous (90% H_2O/10% D_2O) 20 mM sodium phosphate buffer, pH 6.0. Proton shifts were referenced to internal 2,2-dimethyl-2-silapentane-5-sulfonate. Nitrogen shifts were referenced indirectly using a published protocol (28). Urea binding to the I-domain was investigated using a 200 ms mixing time 3D NOESY-HSQC spectrum recorded with 1024 ($^{1}H_N$) × 32 (^{1}H) × 32 (^{15}N) complex points and spectral widths of 8000 × 8000 × 1920 Hz. NMR spectra were processed and analyzed using the FELIX-NMR (San Diego, CA) and CcpNMR (29) software suites.

NSHX

HX experiments were done at 25°C on prelyophilized I-domain samples dissolved in 99.96% D_2O to a final protein concentration of 0.17 mM in 20 mM sodium phosphate, pD 6.0. ^{1}H-^{15}N HSQC spectra to monitor exchange were recorded with 1024 (^{1}H) × 100 (^{15}N) complex points and spectral widths of 7200 × 1404 Hz. To establish that the HX rates were in the EX2 limit, HX data were compared at pH 6.0 and 7.0, both in the absence of urea and at the highest 1.9 M urea concentration used for the NSHX experiments. For the NSHX experiments, HX rates were characterized at urea concentrations of 0, 0.13, 0.23, 0.6, 0.8, 0.9, 1.7, and 1.9 M. For each urea concentration, 25–36 ^{1}H-^{15}N HSQC spectra were collected to monitor HX as a function of the D_2O incubation time. Total experiment times ranged from 1.5 months in the absence of urea to 2 days at the 1.9 M urea concentration.

Exchange rates for each residue were fit to a three-parameter single-exponential decay:

$$I = I_0\, exp(-k_{obs}t) + C, \tag{1}$$

where I_0 is the initial peak intensity, k_{obs} is the observed HX rate, and C is the baseline noise of the spectrum. Fits were done with the program KaleidaGraph version 4.1 (Synergy Software). In the EX2 limit, HX rates can be described by a Gibbs free-energy difference relating the concentrations of closed exchange-resistant and open exchange-susceptible conformations (14,16,30,31):

$$\begin{aligned} G_{HX} &= -RT\, ln(K_{ex}) = -RT\, ln([open]/[closed]) \\ &= -RT\, ln(k_{obs}/k_{int}), \end{aligned} \tag{2}$$

where R is the gas constant, T is the absolute temperature, k_{obs} is the observed HX rate constant, and k_{int} is the intrinsic HX rate, which depends on a number of factors such as pH, temperature, and the sequence of the protein. The k_{int} rates for a given amino acid sequence and set of experimental conditions can be calculated with the SPHERE program online (32).

Temperature and urea dependence of ^{1}HN and ^{15}N chemical shifts

Experiments were performed on 0.6 mM ^{15}N-labeled I-domain samples. For the temperature titration, ^{1}H-^{15}N HSQCs were collected in 5° increments between 5°C and 45°C. For the urea titration, ^{1}H-^{15}N HSQC spectra were collected at nine urea concentrations between 0 and 2.8 M. Based on ^{1}H-^{15}N HSQC spectra and CD spectroscopy, the I-domain remained >90% folded at the largest urea concentration used. ^{1}H-^{15}N HSQC spectra were recorded with 1024 (^{1}H) × 256 (^{15}N) complex points and spectral widths of 8000 × 1920 Hz. Temperature and urea coefficients were determined as the slopes of linear fits of changes in chemical shifts with temperature or urea.

RESULTS

H-bonding and solvent-exchange protection in the I-domain

To better understand the folding properties of the I-domain, given its potential role as an intermolecular chaperone in the

phage P22 coat protein, we probed the stability of H-bonded structure in the I-domain using proton-deuterium HX. Fig. 1 shows representative HX data for the I-domain at pH 6 and 25°C in the absence of urea. Of the 124 residues in the I-domain, 60 have amides that are protected after 4 h in D_2O (Fig. 1 *A*). All protected amides are in the regular H-bonded secondary structure of the I-domain (Fig. 2 *A*). Seven amide protons are not protected but show crosspeaks in the 3D lrHNCO experiment that are consistent with H-bonds (Fig. S1 in the Supporting Material). Of these Q234, F236, V278, and R325 form backbone H-bonds, whereas those of G277, S319, and A326 are H-bonded to side chains or unassigned backbone carbonyls. Another four residues (I228, L281, A285, and T304) are not protected and do not show H-bond couplings in the lrHNCO experiment, but are tentatively assigned to H-bonds based on the I-domain NMR structure (Table S1). In total, 57 protected amides were sufficiently well resolved and long-lived to enable determination of the exchange rates.

After 1 day in D_2O, a subset of 38 amide protons survived, including representatives from all elements of the secondary structure (Fig. 1 *B*). After 6 days of D_2O exchange, a subset of 24 survived. All of the amide protons from helix αi and strands βi and βii were fully exchanged at this stage (Fig. 1 *C*), and strands β1 and βiii had only one remaining amide proton. After 39 days in D_2O, only 11 amide protons persisted (Fig. 1 *D*). With the exception of V313 in strand βii, the remaining amide protons were from strands β2–β5 of the I-domain β-barrel core structure. These protection data suggest that strands β2–β5 of the β-barrel are particularly important for the overall stability of the I-domain.

For thermodynamic information to be obtained, HX rates need to be in the EX2 limit, where exchange is governed by the equilibrium constant relating the populations of exchange-resistant and exchange-susceptible forms of the protein (30,33). By contrast, in the EX1 limit, HX is related to the opening rates that generate HX-susceptible states, and as such does not provide information about the stability of the structure. The hallmark of the EX2 limit is a 10-fold increase in HX rates with each increase of one pH unit above pH ~4.5 (30). To verify that exchange was in the EX2 limit, we compared HX data at pH 6.0 and pH 7.0 as described in Materials and Methods. The logarithms of the HX rates at pH 6.0 were linearly correlated with those at pH 7.0, with a slope of unity and a *y*-intercept that corresponded to the difference of one pH unit between the two data sets (Fig. S2 *A*). These observations are consistent with exchange in the EX2 regime (34). In the presence of urea, HX rates can move out of the EX2 limit as the protein

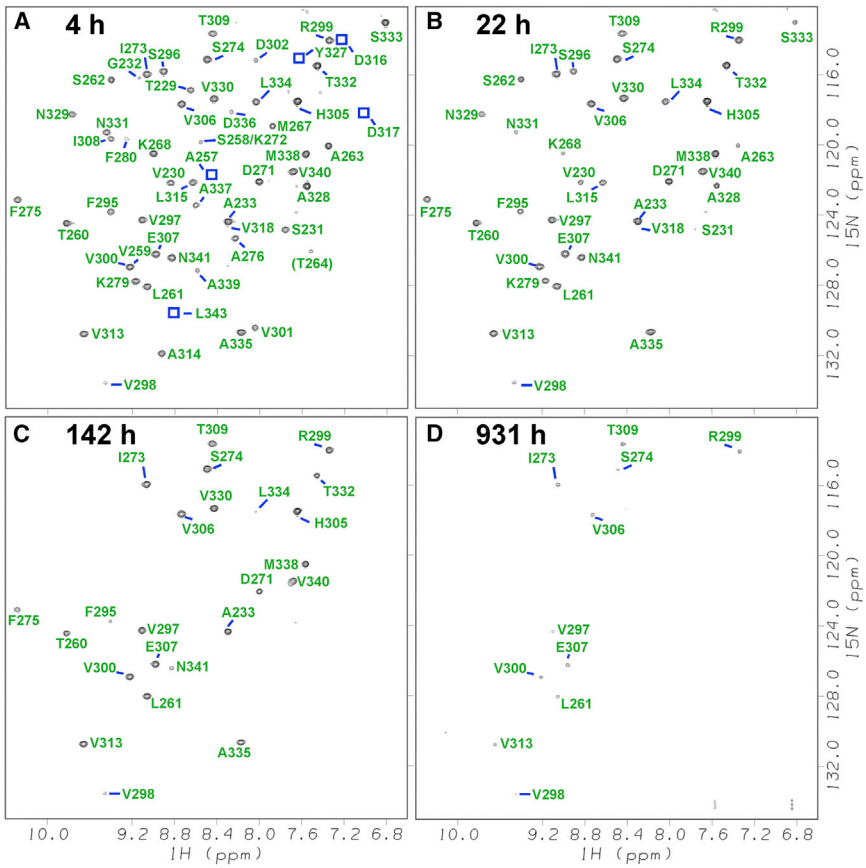

FIGURE 1 Representative ^{1}H-^{15}N HSQC spectra used to monitor HX in the absence of urea. Incubation times in D_2O of (*A*) 4 h, (*B*) 22 h, (*C*) 6 days, and (*D*) 39 days. Signals from protected amide protons are labeled using the published NMR assignments for the I-domain (25). Correlations observed at lower contour levels than shown are indicated by squares in (*A*). The crosspeak for T264 (in parentheses) is folded in the ^{15}N dimension to optimize spectral resolution (the actual ^{15}N chemical shift is 102.84 ppm). To see this figure in color, go online.

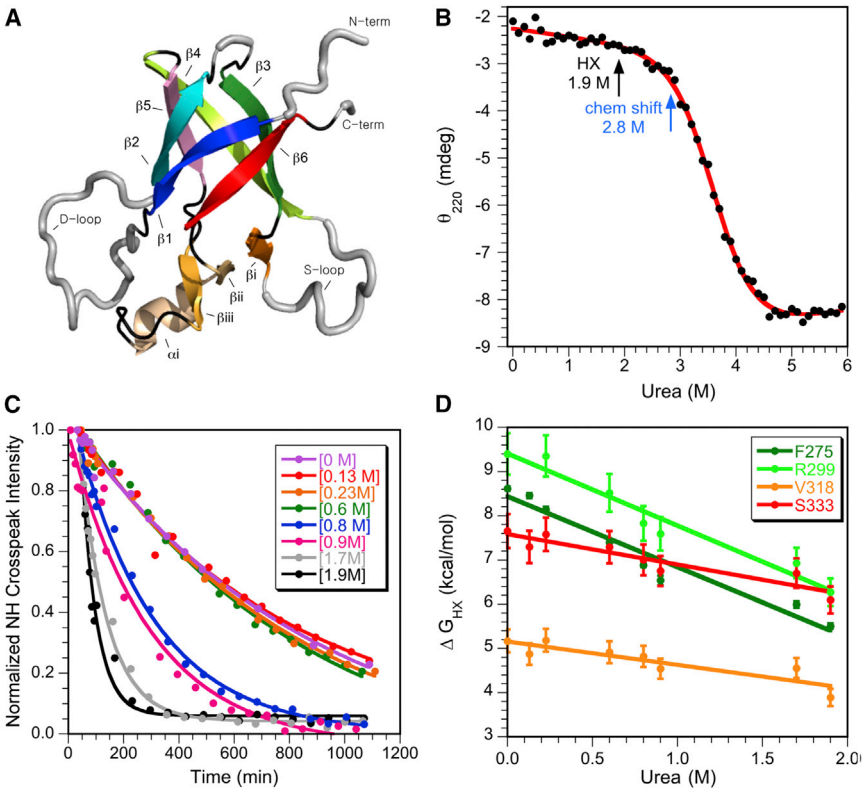

FIGURE 2 Structure, stability, and NSHX of the I-domain. (*A*) NMR structure of the I-domain (8) closest to the ensemble average. The six β-strands of the β-barrel fold are colored blue to red and labeled $\beta1$–$\beta6$. A smaller accessory subdomain consisting of a short α-helix (αi) and three β-strands (βi–βiii) is colored in shades of orange. Flexible segments with backbone ^{15}N S^2 order parameters of <0.85, including the D- and S-loops (8), are depicted with gray tubes. (*B*) Urea unfolding of the I-domain monitored by CD. Thermodynamic parameters for the stability of the I-domain against urea denaturation at pH 6 and 25°C were obtained from a nonlinear least-squares fit of the data (*red curve*) to a six-parameter equation (27), yielding $\Delta G^0_u = 5.8 \pm 0.3$ kcal/mol and $m = 1.6 \pm 0.1$ kcal/mol•M. The arrows show the highest urea concentrations in the native pretransition region used for NSHX (1.9 M) and chemical-shift (2.8 M) studies. (*C*) Representative HX decays for the amide proton of residue S333 at the indicated urea concentrations. The data were fitted to exponential decay functions as detailed in Materials and Methods. (*D*) NSHX isotherms for the indicated residues, showing the urea concentration dependence of ΔG_{HX}. Uncertainties in ΔG_{HX} were propagated from the HX rates as previously described (17).

becomes destabilized (34,35). Consequently, we verified that the exchange rates obeyed the pH dependence expected for the EX2 regime in the presence of 1.9 M urea, the largest urea concentration used in the HX studies (Fig. S2 *B*). We conclude that HX for the I-domain is in the EX2 limit at pH 6.0 over the 0–1.9 M urea concentration range used in this study.

NSHX experiments indicate that the I-domain β-barrel is more stable than the accessory subdomain

Cooperative unfolding, local fluctuations, or both mechanisms can lead to HX. In NSHX experiments, the mechanisms are distinguished through the dependence of ΔG_{HX} (calculated from Eq. 2) on the denaturant concentration (14). Even when a protein is >99% folded (Fig. 2 *B*), cooperative partial or global unfolding reactions will be promoted as the denaturant concentration is increased, whereas noncooperative local fluctuations or breathing mechanisms will not depend on the denaturant concentration (14,16). When both noncooperative and cooperative mechanisms contribute for a given residue at different urea concentrations, HX shows a curved rather than linear urea-concentration isotherm. The exchange rate is initially denaturant independent at low urea concentrations, but it accelerates at larger urea concentrations as cooperative unfolding reactions are promoted by the denaturant (14,16). Fig. 2 *C* shows representative HX data for residue S333 in the I-domain as a function of increasing urea concentration. At all of the urea concentrations used for the NSHX experiments, the protein stays native as monitored by CD (Fig. 2 *B*). The HX rates for S333 increase with the denaturant concentration, indicating that its amide proton exchanges through a cooperative unfolding of the structure around that residue. All of the isotherms measured for the I-domain showed a linear dependence of HX rates on urea concentration, as illustrated by S333 (Fig. 2 *D*), indicating that exchange occurs through either cooperative unfolding or noncooperative fluctuation events at individual sites, but not through both mechanisms.

NSHX isotherms, as exemplified for residue S333 (Fig. 2 *D*), can be used to extract thermodynamic parameters that characterize the energetics of HX. The slope of the isotherm is the m_{HX}-value, a parameter that can be interpreted in terms of the cooperativity of the unfolding reaction (36), or, alternatively, the change in surface-accessible area between the folded exchange-resistant and unfolded exchange-susceptible states (37). The *y*-intercept is the standard-state change in free energy extrapolated to zero denaturant concentration, ΔG^0_{HX}. For residues that have NSHX isotherms with a measurable slope (e.g., nonzero m_{HX}-value), we will use the nomenclature $\Delta G^0_{HX,u}$ to indicate that these residues exchange through a cooperative unfolding process. We use the term $\Delta G^0_{HX,f}$ for residues with exchange rates that are independent of the urea concentration

(e.g., m_{HX} is zero within experimental uncertainty), to indicate that exchange occurs through noncooperative localized breathing fluctuations.

Fig. 3 shows the ΔG^0_{HX}- and m_{HX}-values obtained from NSHX experiments on the I-domain, which are summarized in Table S1. The columns are color-coded as described in the legend for Fig. 3. The gray horizontal bar at 5.8 kcal/mol is the $\Delta G^0_{spec,u}$ obtained from equilibrium denaturation experiments measured by CD spectroscopy. The black horizontal bar at 7.2 kcal/mol is the spectroscopic $\Delta G^0_{spec,u}$-value, with corrections of 0.3 kcal/mol for the increased stability of proteins in D_2O (30), and 1.1 kcal/mol for the proline effect (the I-domain has three *trans* prolines and a *cis* proline at position 310). The proline correction is necessary because prolines have sufficient time to reach their *cis/trans* distribution in a conventional denaturation experiment, but not in an HX experiment (30). Even after these corrections, $\Delta G^0_{spec,u}$ is ~2–3 kcal/mol lower than the largest $\Delta G^0_{HX,u}$-values obtained for some of the residues in the β-barrel (Fig. 3 *A*). An underestimation of $\Delta G^0_{spec,u}$ compared with $\Delta G^0_{HX,u}$ has been observed for other proteins (17,30,34). Possible reasons for this discrepancy include the presence of residual

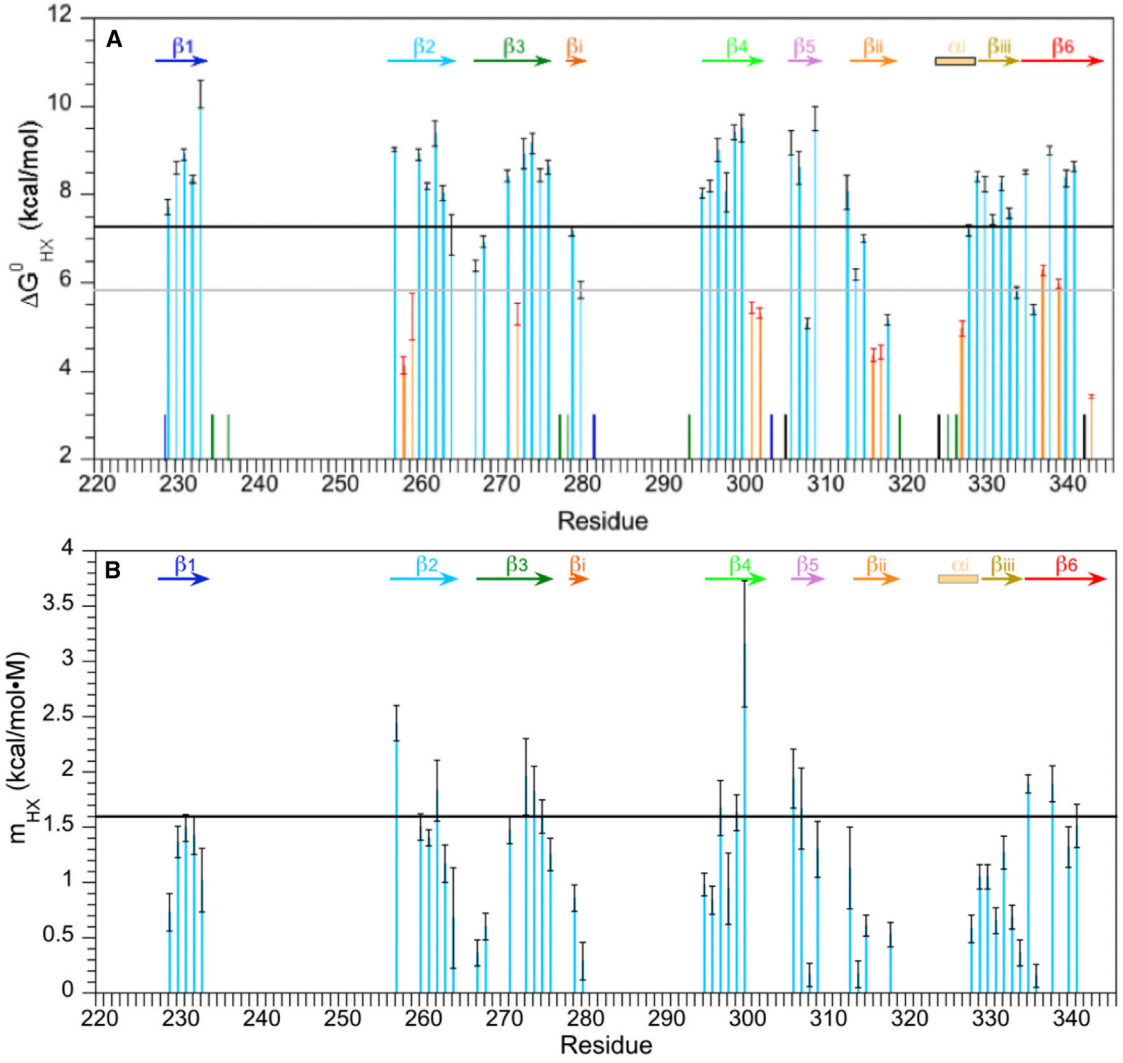

FIGURE 3 Thermodynamic parameters from the NSHX experiments. (*A*) ΔG^0_{HX}-values. Columns in light blue depict residues that show an increase in exchange rates with increasing urea concentration (e.g., see Fig. 2 *C*). The error bars are the mean ± SE of the *y*-intercepts in Fig. 2 *D*. Orange columns depict residues with ΔG_{HX}-values that are constant as a function of urea concentration, within experimental uncertainty. Error bars are mean ± SE. Residues that are H-bonded in the NMR structure but not protected in HX are represented by dark blue bars (arbitrarily set to 3 kcal/mol). Residues with amide protons that are H-bonded according to lrHNCO data but not protected by HX are demarked with green bars. For residues where the protection is too weak to measure, ΔG^0_{HX} is demarked with black bars. The horizontal gray bar indicates the average ΔG^0_u-value of 5.8 ± 0.3 kcal/mol obtained from urea denaturation experiments monitored by CD. The horizontal black bar represents the spectroscopic ΔG^0_u-value of 7.2 kcal/mol after correction for proline isomerization and D_2O contributions (30). (*B*) m_{HX}-values for residues that exchange through a cooperative unfolding mechanism, corresponding to the light-blue $\Delta G^0_{HX,u}$-values in (*A*). The horizontal black bar represents the spectroscopic *m*-value of 1.6 kcal/mol•M. The I-domain secondary structure (Fig. 2 *A*) is shown at the top of each panel.

structure in the denatured state that protects amide protons from HX (30,38), a nonlinear dependence of $\Delta G_{spec,u}$ on denaturant concentration that causes an underestimation of $\Delta G^0_{spec,u}$ when the data are extrapolated to the standard state (34), and averaging of the spectroscopic (e.g., CD) signals from stable and unstable elements of structure when a protein undergoes subglobal unfolding (17,39). Interestingly, if we average over the $\Delta G^0_{HX,u}$-values obtained from the NSHX experiment, we obtain a mean of 8.0 ± 0.2 kcal/mol that is close to the $\Delta G_{spec,u}$-value corrected for the D_2O and proline isomerization effects of 7.2 ± 0.3 kcal/mol. This suggests that $\Delta G_{spec,u}$ corresponds to an average over the range of $\Delta G^0_{HX,u}$-values sampled in the NSHX experiment (17).

The m_{HX}-values from the NSHX experiments on the I-domain are summarized in Fig. 3 *B*. The $\Delta G^0_{HX,u}$- and m_{HX}-values from the NSHX experiment are strongly correlated (Fig. S3), which suggests that the I-domain is undergoing subglobal unfolding reactions (38–40). Thus, the residues that contribute the most to stability are also the ones with the greatest change in solvent exposure during denaturation. In terms of the structure of the I-domain, residues in the β-barrel give the largest $\Delta G^0_{HX,u}$-values, followed by residues in the smaller accessory structure comprised of helix α1 and strands βi–βiii (Figs. 3 *A* and S3). Residues at the ends of the six β-strands that make up the β-barrel also show lower $\Delta G^0_{HX,u}$-values, comparable to those in the accessory motif (Figs. 3 *A* and S3). The residues with no dependence on urea concentration give small $\Delta G^0_{HX,f}$-values, with most of these occurring in the accessory motif and at the ends of strands in the β-barrel (*orange* in Fig. 3 *A*). Because the $\Delta G^0_{HX,u}$ and m_{HX} parameters are correlated, the m_{HX}-values show a similar, albeit more pronounced, structural distribution. The largest m_{HX}-values are in the core of the β-barrel, with those from the accessory motif and strand edges being ~50% smaller (Fig. 3 *B*). Taken together, these results indicate that the β-barrel core of the I-domain corresponds to a more cooperatively stable unit of structure than the accessory subdomain.

^{1}H and ^{15}N amide temperature coefficients distinguish H-bonds

NMR temperature coefficients are the slopes of the linear changes in ^{1}HN or ^{15}N chemical shifts with temperature. Studies of a number of folded proteins (23,41) have indicated that amide protons participating in H-bonds give ^{1}HN temperature coefficients more positive than −4.6 ppb/K, with a predictivity of 85–90% (22–24,41–43). ^{1}HN temperature coefficients also have been reported to be sensitive to H-bond length (24). The predictive power of ^{1}HN temperature coefficients for identifying H-bonds is decreased by other temperature-dependent factors that affect ^{1}HN chemical shifts, such as ring-current effects, conformational averaging, and differences in the magnetic environments of amide protons in α-helix and β-sheet structures (22). To better understand the relationship between H-bonds and temperature-induced chemical-shift changes, we determined both ^{1}HN and ^{15}N temperature coefficients for the I-domain. Representative ^{1}HN and ^{15}N data are shown in Fig. S4, *A* and *B*, and the temperature coefficients of the I-domain are summarized in Table S2.

Of the 93 amide protons that are resolved in the ^{1}H-^{15}N HSQC spectrum of the I-domain, 60 are H-bonded based on independent data from solvent-exchange protection and the 3D-lrHNCO experiment. In Fig. 4, the H-bonded amide protons are indicated by black symbols, and the 33 that are not H-bonded are shown with gray symbols. The ^{1}HN temperature coefficients of the I-domain range from −0.3 to −12.1 ppb/K. Consistent with previously published results (22), 91% of the amide protons that are H-bond donors have ^{1}HN temperature coefficients more positive than −4.6 ppb/K. The eight residues that do not follow this trend are labeled in Fig. 4 *A*. Residues G247, T265, and N287 are false positives, with low temperature coefficients despite the fact that they are not H-bonded. There are several possible explanations for the aberrant behavior of these amide protons. They could be H-bonded to solvent or to moieties that would not be detected in the lrHNCO NMR experiment, such as hydroxyl groups. Residues F275, F280, L334, A339, and I342 are false negatives, with ^{1}HN temperature coefficients more negative than −4.6 ppb/K, even though their amide protons are H-bonded. In fact, F280 has the most negative ^{1}HN temperature coefficient in the I-domain at −12.1 ppb/K, even though it is H-bonded and protected from solvent exchange. A distinguishing feature of the false-negative residues is that they show large $R2_{ex}$ spin-spin relaxation contributions in ^{15}N relaxation measurements (8), suggestive of conformational exchange processes on the microsecond–millisecond timescale. The conformational exchange processes are probably temperature dependent, so the amide proton signals would be shifted with temperature even though they participate in H-bonds.

In addition to ^{1}HN temperature coefficients, we also measured ^{15}N temperature coefficients to evaluate whether they could better discriminate H-bonds (Fig. 4 *B*). The ^{15}N temperature coefficients range from −56 to 26 ppb/K and tend to be positive for H-bonded amide protons (Fig. 4 *B*). Based on the average values of the ^{15}N temperature coefficients for H-bonded and non-H-bonded groups, a cutoff value of −3.7 ppb/K or greater can be used to identify amide protons that are H-bonded. In contrast to the ^{1}HN temperature coefficients, many of the ^{15}N temperature coefficients cluster within experimental uncertainty of the cutoff value. With a cutoff value of −3.7 ppb/K, the ^{15}N temperature coefficients can discriminate H-bonded from non-H-bonded amide protons with an accuracy of 80% (73 of 90 residues). The ^{1}HN and ^{15}N temperature coefficients are only weakly correlated (Fig. S5 *A*), indicating that they

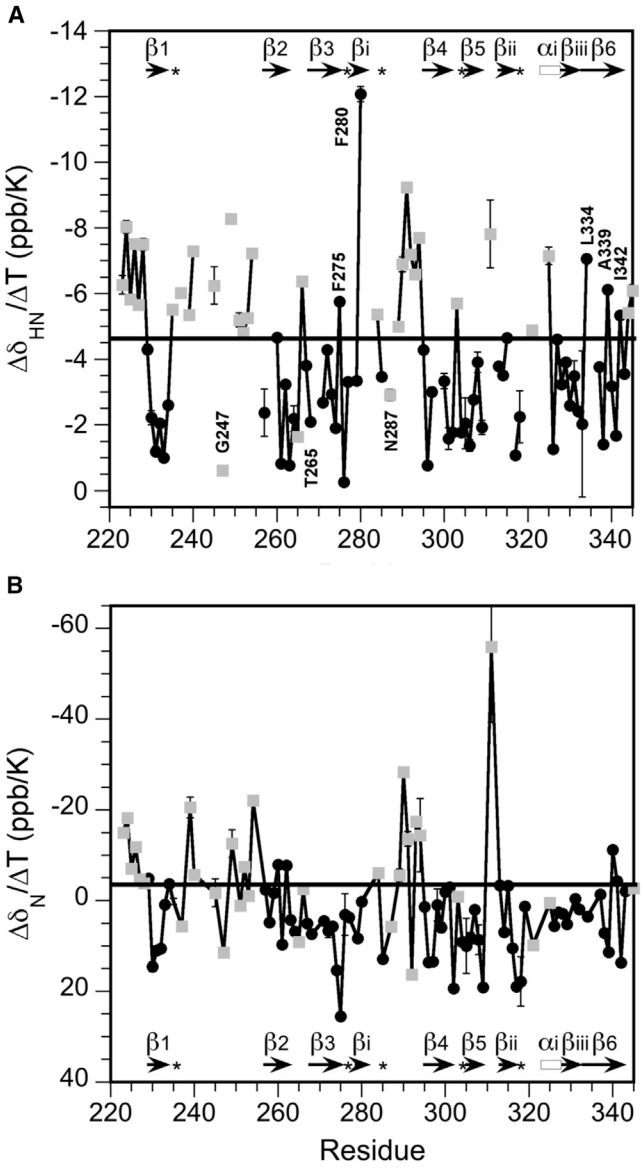

FIGURE 4 Temperature dependence of I-domain ^{1}HN and ^{15}N chemical shifts. (*A*) ^{1}HN temperature coefficients. The horizontal bar shows the published −4.6 ppb/K cutoff for H-bonded amide protons (22,23). Residues with aberrant temperature coefficients are indicated. (*B*) ^{15}N temperature coefficients. The horizontal bar shows the −3.7 ppb/K cutoff for H-bonded amide protons described in this work. H-bonded residues are shown in black and residues that are not H-bonded are in gray. The secondary structure of the I-domain is shown, with the * symbols indicating residues with H-bonded amide protons that are not part of regular secondary structure. The mean ± SE is shown for all data points, but in some cases is smaller than the symbols.

depend on factors other than H-bonding. We hypothesized that a combination of the two parameters could improve the accuracy of H-bond identification. One possible approach is to consider only residues where ^{1}HN and ^{15}N temperature coefficients agree. This results in an improved accuracy of 96% (three amide protons incorrectly predicted out of 71), but requires one to discard the data for 22 amide protons (24% of the total). Moreover, amide protons that are not H-bonded and yet have large temperature coefficients are a major limitation with the ^{15}N data (Fig. 4 *B*). An alternative approach is to recognize that the ^{1}HN data are more accurate than the ^{15}N data. Thus, we chose a method in which ^{1}HN temperature coefficients were primarily used to predict H-bonds. If we identified a conflict between the ^{1}HN and ^{15}N temperature coefficients, the ^{15}N temperature coefficient superseded the ^{1}HN temperature coefficient only if it was larger than 10 ppb/K and the ^{1}HN temperature coefficient was greater than −7 ppb/K. In these cases, the amide proton was assigned as H-bonded. With this approach, only five amide protons (G247, T265, F280, N287, and L334) were incorrectly predicted as compared with our HX and lrHNCO data, resulting in an accuracy of 95% for the 93 observable amide protons. In summary, the ^{1}HN temperature coefficients achieve an accuracy of ~91%, and this can be further improved to 95% by considering data for residues with large positive ^{15}N temperature coefficients.

We observed a weak negative correlation between ^{1}HN temperature coefficients and N-O atom distance across H-bonds, calculated from $^{3}J_{NC'}$ couplings (19,44), in the 3D lrHNCO spectrum (Fig. S5 *B*) that is consistent with reports that ^{1}HN temperature coefficients increase with decreasing H-bond length (22,24). Besides H-bonding, we found a weak positive correlation between ^{1}HN temperature coefficients and S^2 order parameters obtained from ^{15}N relaxation measurements (Fig. S5 *C*). The correlation probably occurs because amide protons in the rigid portions of the I-domain tend to be involved in regular H-bonded secondary structure, whereas those in disordered segments are not H-bonded. The ^{1}HN temperature coefficients show no relationship with the ΔG^0_{HX}-values from the NSHX experiments. The ΔG^0_{HX}-values depend on the stability and deformability of cooperative units of structure rather than the properties of individual H-bonds.

Urea binding by the I-domain

To probe the process by which urea causes the unfolding of proteins, we next examined the urea-concentration dependence of I-domain ^{1}HN and ^{15}N chemical shifts up to a denaturant concentration of 2.8 M, where the protein remains predominantly folded (Fig. 2 *B*). Representative data for six I-domain residues are shown in Fig. S4, *C* and *D*. Chemical-shift changes induced by urea showed a mixture of linear and nonlinear responses. Sigmoidal and, more rarely, hyperbolic chemical-shift changes with urea were observed for 22 of 102 ^{1}HN signals and 35 of 98 ^{15}N resonances, as illustrated by residues V239, L261, Q291, and I308 in Fig. S4, *C* and *D*. Residues with ^{1}H or ^{15}N resonances showing a curved dependence on urea concentration cluster mainly to the disordered D- and S-loops, but some are found in regions of regular secondary

structure, with the accessory motif having a larger proportion than the β-barrel. Parameters from fits of the nonlinear urea titration curves to sigmoidal and hyperbolic binding equations are given in Table S3. Because most residues showed a linear relationship, and for consistency with the temperature experiments, we also fitted all ^{1}HN and ^{15}N signals to straight lines to obtain urea coefficients, i.e., the slopes of the chemical-shift changes as a function of urea concentration (see Fig. S6 and Table S2). Whereas the slopes of ^{1}HN shift changes with temperature were exclusively negative, the urea titration experiments gave both positive and negative slopes. In contrast to the temperature coefficients, the ^{1}HN and ^{15}N urea coefficients showed no significant differences between residues that were H-bonded and those that were not. Moreover, the ^{1}HN and ^{15}N urea coefficients were not correlated to the ^{1}HN temperature coefficients, which were sensitive to H-bonding (Fig. S5 *D*). These observations indicate that the ^{1}H and ^{15}N urea coefficients depend on factors other than H-bonding; rather, the urea coefficients seem to be a function of structural disorder. Some of the largest urea coefficients occurred in the disordered loop segments of the protein that also showed nonlinear behavior in chemical-shift changes due to increased urea.

The curved or sigmoidal chemical-shift responses to urea concentration are suggestive of weak urea-binding equilibria. To test this hypothesis, we recorded a 3D NOESY-HSQC spectrum on the I-domain in the presence of 2.8 M urea, where the protein is still predominantly folded (Fig. 2 *B*). NOEs to urea at 5.76 ppm were seen for 31 of 112 resolved amide protons. Residues with NOEs to urea occurred mostly in the unfolded segments of the protein, i.e., the chain termini together with the D- and S-loops. Although there is no one-to-one correspondence, these regions also show the largest fractions of residues with sigmoidal urea titration curves (Tables S2 and S3) along with the largest ^{1}HN and ^{15}N urea coefficients (Fig. S6). In addition to the disordered segments, two residues from the accessory motif and five residues from the six-stranded β-barrel show NOEs to urea. These occur at the ends of elements of the regular secondary structure (Table S2). Representative data from the 3D NOESY-HSQC for a 10-residue segment in the I-domain are shown in Fig. S7. The data suggest that there are specific binding sites in the I-domain for urea. Most of these occur in the disordered segments of the I-domain, but some are located at the ends of elements of the regular secondary structure.

DISCUSSION

The center of the I-domain β-barrel is the most stably folded

The core of the six-stranded β-barrel motif is the most stable structural unit in the I-domain, as indicated by NSHX experiments. This is followed by the structurally nonconserved accessory subdomain, consisting of a short α-helix and three short strands of β-sheet. The ends of the β-strands in the β-barrel have stabilities comparable to those of the accessory subdomain. H-bonds outside elements of the regular secondary structure are the least stable, showing no solvent protection (Table S1).

The stability hierarchy of the I-domain is summarized in Fig. 5. Note that there are small one- to two-residue differences in the limits of the secondary structure elements from the published NMR structure in Fig. 5 *A* (8). These occur because β-strands and α-helices are defined by both H-bonds and backbone dihedral angles in the NMR structure, whereas in this work we are considering only H-bonds. The most significant difference is that strand βiii in the accessory domain appears to be contiguous with strand β6 in the β-barrel, running from N329 to L343 (Table S2). By contrast, in the NMR structure, strand βiii consists of residues N329–T332 and strand β6 consists of A335–L343, with residues S333–L334 comprising a two-residue break of irregular structure. Fig. 5 *B* shows the I-domain H-bonds with amide protons sufficiently protected to measure HX rates ($\Delta G^{0}_{HX} > 3.4$ kcal/mol). Segments of the I-domain that have little or no protection from HX include

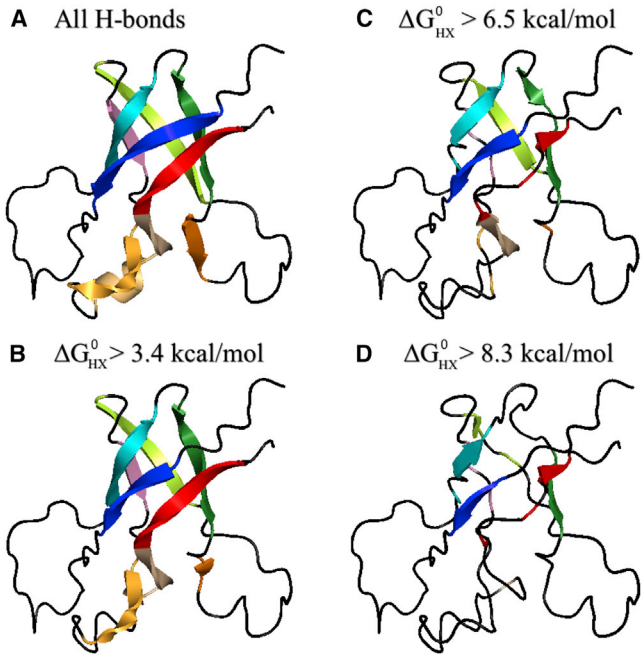

FIGURE 5 Hierarchy of ΔG^{0}_{HX}-values mapped onto the I-domain structure: (*A*) all H-bonds, (*B*) $\Delta G^{0}_{HX} > 3.4$ kcal/mol, (*C*) $\Delta G^{0}_{HX} > 6.5$ kcal/mol, and (*D*) $\Delta G^{0}_{HX} > 8.3$ kcal/mol. The coloring scheme is the same as in Fig. 2 *A*, but the secondary structure limits differ somewhat because all H-bonds are considered not just those with dihedral angles for regular secondary structure. Secondary structure elements, drawn if the stated ΔG^{0}_{HX} stability criteria are satisfied for a segment of two or more residues, are progressively reduced to show H-bonds with stabilities above the indicated thresholds.

most of helix α1 and parts of strand βi in the accessory domain, as well as the N- and C-termini of β-barrel strands β1 and β6. Fig. 5 *C* shows the subset of amide protons with $\Delta G^0_{HX} > 6.5$ kcal/mol. The β-barrel segment of the I-domain, except for the N-termini of strands 1 and 6, shows amide proton protection above this threshold. Most of the amide protons from the accessory subdomain, except for strand βiii, fall below the ΔG^0_{HX} stability threshold of 6.5 kcal/mol. Fig. 5 *D* shows the most stable amide protons in the I-domain, with $\Delta G^0_{HX} > 8.5$ kcal/mol. These occur in the center of the five-stranded β-barrel structure.

A general correlation between solvent-exchange protection and the number of Cα-Cα contacts has been observed for many proteins (45). This probably reflects the fact that portions of the structure with the largest number of interresidue interactions are the most difficult to deform in the unfolding transitions that allow HX. NSHX studies of three proteins from the OB-fold family, a common protein fold based on a five-stranded β-barrel (46), showed a positive correlation between stability described by the NSHX ΔG^0_{HX} parameters and the density of Cα-Cα contacts in the structure (31). Thus, the largest stability against HX occurs in the conserved five-stranded β-barrel fold (31,47). A bioinformatics analysis of 95 protein domains that share the OB-fold motif showed that the conserved five-stranded β-barrel fold had a higher density of Cα-Cα contacts than the nonconserved secondary structure (47). Based on these results, a model of protein structure evolution was proposed in which novel structural features develop at the peripheries of conserved structure motifs (47). Our NSHX results regarding the I-domain also support this model, inasmuch as the structurally conserved β-barrel was more stable against HX than the accessory domain, which does not have a conserved tertiary structure in structurally homologous proteins (8). Although the results were not as pronounced as for the OB-fold proteins, on a per-residue basis, the ΔG^0_{HX}-values of the I-domain correlated with the number of Cα-Cα distance contacts per residue, averaged over a window of five residues (R-value = 0.40, $\rho < 0.002$ for $n = 55$). Thus, the stability of a structure in the I-domain is related to its deformability, i.e., the number of distance contacts that need to be disrupted to unfold the structure.

Interaction of urea with regions of the I-domain

Equilibrium denaturation experiments monitored by optical spectroscopy (e.g., see Fig. 2 *B*) often give nonzero slopes for the pre- and posttransition regions. These slopes have been attributed to nonspecific solvent effects (48), although in some cases structural transitions have been described in denaturation pretransition regions (49,50). Compared with optical spectroscopy, NMR offers the advantage of atomic resolution. Whereas ^{1}HN temperature coefficients more positive than −4.6 ppb/K identify H-bonds in the I-domain with an accuracy of ~90% (Fig. 4 *A*), the urea-concentration dependence of ^{1}H and ^{15}N chemical shifts shows no relationship with H-bonding (Fig. S6). Linear chemical-shift changes with increasing urea concentration are seen for the majority of residues in the I-domain. Approximately 45 of 103 residues (44%), however, show sigmoidal or, more rarely, hyperbolic changes in ^{1}H and/or ^{15}N chemical shifts with urea concentration. Representative linear and sigmoidal curves are shown in (Fig. S4, *C* and *D*). The residues with nonlinear curves are located mostly in the disordered loops and at the interface between disordered and structured segments, but some are also found in the folded core. We fit the ^{1}H and ^{15}N signals with a nonlinear dependence on urea concentration to hyperbolic or sigmoidal binding curves to extract K_d-values for urea binding and *n*-values (Hill coefficients) describing the cooperativity of urea binding. The fitting parameters are given in Table S3. The majority of the nonlinear curves (88%) are sigmoidal rather than hyperbolic, indicating cooperative urea binding. Cooperativity implies that as one urea molecule binds, it distorts the structure to make additional urea-binding sites available. The urea binding data in Table S3 show differences between ordered and disordered segments of the I-domain, and smaller differences between the accessory subdomain and the six-stranded β-barrel motif. The subset of disordered residues, at the chain termini and D- and S-loops, have S^2 order parameters from ^{15}N relaxation experiments that are <0.85 (8). Considering the disordered subset, the K_d-values for urea binding range from 0.4 to 1.2 M, and the *n*-values range from 1 to 3.5. By contrast, for the ordered subset with S^2 order parameters of >0.85, the K_d-values range from 0.6 to 1.8 M urea, and the *n*-values range from 1 to 11. The two subsets of residues show differences in the mean values of the K_d for urea binding (0.9 ± 0.2 M for flexible, 1.1 ± 0.2 for rigid, $\rho = 0.006$) and in the *n*-values describing the cooperativity of urea binding (2.3 ± 0.5 M for flexible, 3.8 ± 2.2 for rigid, $\rho = 0.01$). Thus, the ordered parts of the I-domain bind urea more cooperatively, and the binding requires larger concentrations of urea than the disordered segments. Within the subset of ordered residues, we also see significant differences ($\rho = 0.02$) between the mean K_d-values of sites in the accessory subdomain (1.0 ± 0.2) and in the six-stranded β-barrel (1.2 ± 0.2). Thus, the β-barrel binds urea the least readily, with the accessory subdomain having an intermediate avidity compared with the disordered segments. The differences in *n*-values between the β-barrel and the accessory subdomain are not significant, probably because urea binding disrupts similarly sized secondary structure elements.

Further evidence for the presence of multiple distinct urea-binding sites comes from a 3D NOESY-HSQC spectrum collected in the presence of 2.8 M urea. NOEs to urea have been previously observed for unfolded proteins (50,51) and the folded state of bovine pancreatic trypsin inhibitor, where urea binding occurred at specific crevices and pockets on the protein surface (52). In the I-domain, NOEs

to urea are seen primarily in the unstructured loops, in the accessory subdomain, and at the edges of the strands that make up the β-barrel core of the protein structure (Table S2). The regions of the proteins that show NOEs to urea also show the largest proportion of sigmoidal chemical-shift responses and the largest chemical-shift changes with urea (Fig. S6). Fig. 6 shows the structure of the I-domain color-coded according to the ΔG^0_{HX} (Fig. 6 *A*) and m_{HX} (Fig. 6 *B*) obtained from the NSHX experiments. Residues that show NOEs to urea are shown as spheres in Fig. 6 *A* and typically occur near the portions of the I-domain structure that have the smallest ΔG^0_{HX}- and m_{HX}-values in the NSHX experiments. These data suggest that the lower stability in NSHX experiments may be linked to the higher solvent accessibility and the higher affinity for urea binding of these sites.

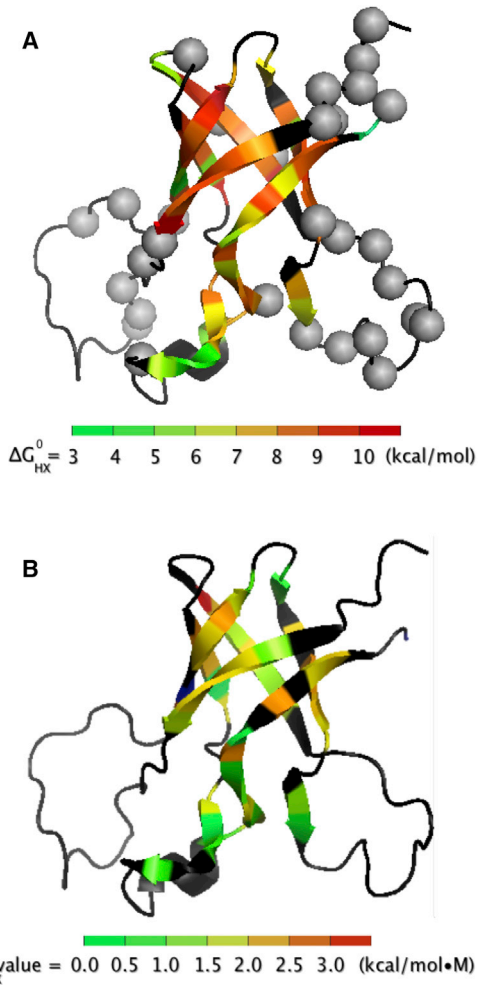

FIGURE 6 Mapping of ΔG^0_{HX}- and m_{HX}-values, and residues that show NOEs to urea on the I-domain structure. (*A*) ΔG^0_{HX}-values mapped according to the indicated color gradient. Black segments are those for which there are no data. Note that the figure does not distinguish between residues that exchange through a $\Delta G^0_{HX,u}$ and $\Delta G^0_{HX,f}$ mechanism. Residues that show amide proton NOEs to urea are depicted with gray spheres. (*B*) NSHX m_{HX}-values with the indicated color gradient.

A proposed mechanism for urea denaturation of proteins

There are various models for how urea denatures proteins. In one model, urea is suggested to unfold proteins indirectly by disrupting the structure of water (53). Recent experimental evidence and theoretical work, however, suggest that the structure of water does not change to any great extent in the presence of urea (54,55). In an alternative model, urea is proposed to interact directly with the protein, although whether the interactions are with hydrophobic side chains, the polar backbone, or both remains unresolved (55–57). Our results are consistent with a direct interaction between urea and the I-domain at the urea concentrations in the denaturation pretransition region used in this study. We cannot exclude a change in mechanism for the major cooperative denaturation transition that occurs at ~3.5 M urea (Fig. 2 *B*). In the pretransition region, urea appears to bind preferentially to the disordered S- and D-loops of the I-domain, suggesting that it has a higher avidity for unstructured polypeptides. As the urea concentration increases, the unfolded state will be increasingly favored through the law of mass action. If there were no differences in the interactions of urea with different segments of the protein, unfolding would appear as a two-state transition even in an NSHX experiment. Conversely, if some segments bind urea preferentially, these would be the first to unfold as observed in the NSHX experiments. This could occur even at a urea concentration where unfolding is undetectable by conventional spectroscopic methods but observable by HX. In the I-domain, as in other proteins, the first segments to unfold are those with the lowest Cα-Cα contact densities, which are likely also the most accessible to urea.

If urea promotes unfolding by binding to specific sites on the protein, this raises the question of whether unfolding differs with different types of denaturants. For the I-domain, this can be ruled out because the NSHX isotherms as a function of urea concentration are all linear. Linear extrapolation of the NSHX isotherms to the standard state gives ΔG^0_{HX}-values very similar to the ΔG_{HX}-values measured in D_2O in the absence of urea. For proteins that exhibit nonlinear NSHX isotherms, unfolding that is specific to the type of denaturant could be more difficult to rule out, but in principle, one could address this issue by performing NSHX experiments with different types of denaturants.

SUPPORTING MATERIAL

Seven figures and three tables are available at http://www.biophysj.org/biophysj/supplemental/S0006-3495(15)01167-4.

AUTHOR CONTRIBUTIONS

R.L.N. and L.C.R.F. produced the I-domain samples. R.L.N., L.C.R.F., and A.T.A. performed NMR experiments and analyzed the data. L.C.R.F. did

the NSHX experiments and R.L.N. did the temperature and urea titration experiments. A.T.A. and C.M.T. wrote the article. All authors discussed the results and commented on the article.

ACKNOWLEDGMENTS

We thank Alex Rizzo and Mark Maciejewski for the lrHNCO data on the I-domain.

This work was supported by NIH grant R01 GM076661 to C.M.T. and a supplement to C.M.T. and A.T.A.

REFERENCES

1. Suhanovsky, M. M., and C. M. Teschke. 2015. Nature's favorite building block: deciphering folding and capsid assembly of proteins with the HK97-fold. *Virology.*:479–480:487–497.
2. Klose, T., and M. G. Rossmann. 2014. Structure of large dsDNA viruses. *Biol. Chem.* 395:711–719.
3. Rossmann, M. G. 2013. Structure of viruses: a short history. *Q. Rev. Biophys.* 46:133–180.
4. Wikoff, W. R., L. Liljas, …, J. E. Johnson. 2000. Topologically linked protein rings in the bacteriophage HK97 capsid. *Science.* 289:2129–2133.
5. Suhanovsky, M. M., and C. M. Teschke. 2011. Bacteriophage P22 capsid size determination: roles for the coat protein telokin-like domain and the scaffolding protein amino-terminus. *Virology.* 417:418–429.
6. Chen, D. H., M. L. Baker, …, W. Chiu. 2011. Structural basis for scaffolding-mediated assembly and maturation of a dsDNA virus. *Proc. Natl. Acad. Sci. USA.* 108:1355–1360.
7. Parent, K. N., R. Khayat, …, T. S. Baker. 2010. P22 coat protein structures reveal a novel mechanism for capsid maturation: stability without auxiliary proteins or chemical crosslinks. *Structure.* 18:390–401.
8. Rizzo, A. A., M. M. Suhanovsky, …, C. M. Teschke. 2014. Multiple functional roles of the accessory I-domain of bacteriophage P22 coat protein revealed by NMR structure and cryoEM modeling. *Structure.* 22:830–841.
9. Tripler, T. N., M. W. Maciejewski, …, A. T. Alexandrescu. 2015. NMR assignments for the insertion domain of bacteriophage CUS-3 coat protein. *Biomol. NMR Assign.* 9:333–336.
10. Parent, K. N., J. Tang, …, T. S. Baker. 2014. Three-dimensional reconstructions of the bacteriophage CUS-3 virion reveal a conserved coat protein I-domain but a distinct tailspike receptor-binding domain. *Virology.* 464-465:55–66.
11. Suhanovsky, M. M., and C. M. Teschke. 2013. An intramolecular chaperone inserted in bacteriophage P22 coat protein mediates its chaperonin-independent folding. *J. Biol. Chem.* 288:33772–33783.
12. Gordon, C. L., and J. King. 1993. Temperature-sensitive mutations in the phage P22 coat protein which interfere with polypeptide chain folding. *J. Biol. Chem.* 268:9358–9368.
13. Ma, B., C. J. Tsai, and R. Nussinov. 2000. Binding and folding: in search of intramolecular chaperone-like building block fragments. *Protein Eng.* 13:617–627.
14. Bai, Y., T. R. Sosnick, …, S. W. Englander. 1995. Protein folding intermediates: native-state hydrogen exchange. *Science.* 269:192–197.
15. Bai, Y., J. S. Milne, …, S. W. Englander. 1993. Primary structure effects on peptide group hydrogen exchange. *Proteins.* 17:75–86.
16. Chamberlain, A. K., T. M. Handel, and S. Marqusee. 1996. Detection of rare partially folded molecules in equilibrium with the native conformation of RNaseH. *Nat. Struct. Biol.* 3:782–787.
17. Alexandrescu, A. T., V. A. Jaravine, …, F. P. Lamour. 1999. NMR hydrogen exchange of the OB-fold protein LysN as a function of denaturant: the most conserved elements of structure are the most stable to unfolding. *J. Mol. Biol.* 289:1041–1054.
18. Cordier, F., and S. Grzesiek. 1999. Direct observation of hydrogen bonds in proteins by interresidue 3HJNC' scalar couplings. *J. Am. Chem. Soc.* 121:1601–1602.
19. Alexandrescu, A. T., D. R. Snyder, and F. Abildgaard. 2001. NMR of hydrogen bonding in cold-shock protein A and an analysis of the influence of crystallographic resolution on comparisons of hydrogen bond lengths. *Protein Sci.* 10:1856–1868.
20. Jaravine, V. A., A. T. Alexandrescu, and S. Grzesiek. 2001. Observation of the closing of individual hydrogen bonds during TFE-induced helix formation in a peptide. *Protein Sci.* 10:943–950.
21. Cornilescu, G., J. S. Hu, and A. Bax. 1999. Identification of the hydrogen bonding network in a protein by scalar couplings. *J. Am. Chem. Soc.* 121:2949–2950.
22. Cierpicki, T., and J. Otlewski. 2001. Amide proton temperature coefficients as hydrogen bond indicators in proteins. *J. Biomol. NMR.* 21:249–261.
23. Baxter, N. J., and M. P. Williamson. 1997. Temperature dependence of 1H chemical shifts in proteins. *J. Biomol. NMR.* 9:359–369.
24. Hong, J., Q. Jing, and L. Yao. 2013. The protein amide ^{1}H(N) chemical shift temperature coefficient reflects thermal expansion of the N-H$\cdots$O=C hydrogen bond. *J. Biomol. NMR.* 55:71–78.
25. Rizzo, A. A., L. C. Fraser, …, A. T. Alexandrescu. 2013. NMR assignments for the telokin-like domain of bacteriophage P22 coat protein. *Biomol. NMR Assign.* 7:257–260.
26. Pace, C. N. 1986. Determination and analysis of urea and guanidine hydrochloride denaturation curves. *Methods Enzymol.* 131:266–280.
27. Santoro, M. M., and D. W. Bolen. 1988. Unfolding free energy changes determined by the linear extrapolation method. 1. Unfolding of phenylmethanesulfonyl alpha-chymotrypsin using different denaturants. *Biochemistry.* 27:8063–8068.
28. Wishart, D. S., C. G. Bigam, …, B. D. Sykes. 1995. 1H, 13C and 15N chemical shift referencing in biomolecular NMR. *J. Biomol. NMR.* 6:135–140.
29. Vranken, W. F., W. Boucher, …, E. D. Laue. 2005. The CCPN data model for NMR spectroscopy: development of a software pipeline. *Proteins.* 59:687–696.
30. Bai, Y., J. S. Milne, …, S. W. Englander. 1994. Protein stability parameters measured by hydrogen exchange. *Proteins.* 20:4–14.
31. Watson, E., W. M. Matousek, …, A. T. Alexandrescu. 2007. Partially folded states of staphylococcal nuclease highlight the conserved structural hierarchy of OB-fold proteins. *Biochemistry.* 46:9484–9494.
32. Zhang, Y.-Z. 1995. Protein and peptide structure and interactions studied by hydrogen exchange and NMR. PhD thesis. University of Pennsylvania, Philadelphia.
33. Englander, S. W., L. Mayne, …, T. R. Sosnick. 1997. Hydrogen exchange: the modern legacy of Linderstrøm-Lang. *Protein Sci.* 6:1101–1109.
34. Yi, Q., M. L. Scalley, …, D. Baker. 1997. Characterization of the free energy spectrum of peptostreptococcal protein L. *Fold. Des.* 2:271–280.
35. Clarke, J., and A. R. Fersht. 1996. An evaluation of the use of hydrogen exchange at equilibrium to probe intermediates on the protein folding pathway. *Fold. Des.* 1:243–254.
36. Carra, J. H., and P. L. Privalov. 1996. Thermodynamics of denaturation of staphylococcal nuclease mutants: an intermediate state in protein folding. *FASEB J.* 10:67–74.
37. Shortle, D. 1995. Staphylococcal nuclease: a showcase of m-value effects. *Adv. Protein Chem.* 46:217–247.
38. Cortajarena, A. L., S. G. Mochrie, and L. Regan. 2008. Mapping the energy landscape of repeat proteins using NMR-detected hydrogen exchange. *J. Mol. Biol.* 379:617–626.
39. Liang, X., G. I. Lee, and S. R. Van Doren. 2006. Partially unfolded forms and non-two-state folding of a beta-sandwich: FHA domain from Arabidopsis receptor kinase-associated protein phosphatase. *J. Mol. Biol.* 364:225–240.

40. Llinás, M., B. Gillespie, …, S. Marqusee. 1999. The energetics of T4 lysozyme reveal a hierarchy of conformations. *Nat. Struct. Biol.* 6:1072–1078.

41. Cierpicki, T., I. Zhukov, …, J. Otlewski. 2002. Hydrogen bonds in human ubiquitin reflected in temperature coefficients of amide protons. *J. Magn. Reson.* 157:178–180.

42. Bouvignies, G., P. Vallurupalli, …, L. E. Kay. 2011. Measuring 1HN temperature coefficients in invisible protein states by relaxation dispersion NMR spectroscopy. *J. Biomol. NMR.* 50:13–18.

43. Dyson, H. J., M. Rance, …, P. E. Wright. 1988. Folding of immunogenic peptide fragments of proteins in water solution. I. Sequence requirements for the formation of a reverse turn. *J. Mol. Biol.* 201:161–200.

44. Cornilescu, G., B. E. Ramirez, …, A. Bax. 1999. Correlation between 3hJNC' and hydrogen-bond length in proteins. *J. Am. Chem. Soc.* 121:6275–6279.

45. Bahar, I., A. Wallqvist, …, R. L. Jernigan. 1998. Correlation between native-state hydrogen exchange and cooperative residue fluctuations from a simple model. *Biochemistry.* 37:1067–1075.

46. Murzin, A. G. 1993. OB(oligonucleotide/oligosaccharide binding)-fold: common structural and functional solution for non-homologous sequences. *EMBO J.* 12:861–867.

47. Guardino, K. M., S. R. Sheftic, …, A. T. Alexandrescu. 2009. Relative stabilities of conserved and non-conserved structures in the OB-fold superfamily. *Int. J. Mol. Sci.* 10:2412–2430.

48. Ahmad, F. 1984. Free energy changes in denaturation of ribonuclease A by mixed denaturants. Effects of combinations of guanidine hydrochloride and one of the denaturants lithium bromide, lithium chloride, and sodium bromide. *J. Biol. Chem.* 259:4183–4186.

49. Stelea, S. D., and T. A. Keiderling. 2002. Pretransitional structural changes in the thermal denaturation of ribonuclease S and S protein. *Biophys. J.* 83:2259–2269.

50. Gupta, S., and S. Bhattacharjya. 2014. NMR characterization of the near native and unfolded states of the PTB domain of Dok1: alternate conformations and residual clusters. *PLoS One.* 9:e90557.

51. Dötsch, V., G. Wider, …, K. Wüthrich. 1995. Interaction of urea with an unfolded protein. The DNA-binding domain of the 434-repressor. *FEBS Lett.* 366:6–10.

52. Liepinsh, E., and G. Otting. 1994. Specificity of urea binding to proteins. *J. Am. Chem. Soc.* 116:9670–9674.

53. Frank, H. S., and F. Franks. 1968. Structural approach to the solvent power of water for hydrocarbons; urea as a structure breaker. *J. Chem. Phys.* 48:4746–4757.

54. Carr, J. K., L. E. Buchanan, …, J. L. Skinner. 2013. Structure and dynamics of urea/water mixtures investigated by vibrational spectroscopy and molecular dynamics simulation. *J. Phys. Chem. B.* 117:13291–13300.

55. Hua, L., R. Zhou, …, B. J. Berne. 2008. Urea denaturation by stronger dispersion interactions with proteins than water implies a 2-stage unfolding. *Proc. Natl. Acad. Sci. USA.* 105:16928–16933.

56. Makhatadze, G. I., and P. L. Privalov. 1992. Protein interactions with urea and guanidinium chloride. A calorimetric study. *J. Mol. Biol.* 226:491–505.

57. Almarza, J., L. Rincon, …, F. Brito. 2009. Molecular mechanism for the denaturation of proteins by urea. *Biochemistry.* 48:7608–7613.